Int. J. Heat Mass Transfer. Vol. 31, No. 10, pp. 2023–2032, 1988
Printed in Great Britain

0017-9310/88 $3.00+0.00

Minimum-dissipation heat removal by scale-matched flow destabilization

H. KOZLU, B. B. MIKIC and A. T. PATERA
Department of Mechanical Engineering, Massachusetts Institute of Technology, Cambridge, MA 02139, U.S.A.

(*Received* 21 *September* 1987 *and in final form* 1 *March* 1988)

Abstract—Minimum-dissipation convective heat removal from a wall to a flowing fluid stream by scale-matched flow destabilization is considered. A universal scaling for the optimization problem is developed, and it is shown from Reynolds analogy–hydrodynamic stability arguments that the dissipation-minimizing transport solution corresponds to flow destabilization at a Reynolds number (*and associated spatial scale*) that increases (*decreases*) with increasing thermal load. The significant dissipation savings possible through optimization are demonstrated in a sample optimization study for heat transfer in a channel based on experimental data for several enhancement procedures. The optimizing transport enhancement scheme is shown to proceed from macroscale eddy promoters to microgroove roughness elements with increasing thermal load, thus verifying the validity of the scale-matched destabilization theory.

1. INTRODUCTION

THE PROBLEM of removal of heat from a surface to a flowing fluid stream arises in a large number of important technological systems. It is clear that in any particular application the necessary heat transfer can be effected in a number of different ways, and thus for the design problem to be well posed a cost function must be introduced that reflects the constraints and goals of the overall system. We address here the optimization problem corresponding to maintaining a *fixed* thermal load while *minimizing* shear stress, pressure drop, and viscous dissipation (pumping power).

The choice of momentum–transport–penalty heat transfer optimization is motivated by the following facts: excessive shear stress can adversely effect structural integrity (e.g. in biomedical applications [1]); excessive pressure drop can result in large structural loads leading to failure or significant cost of materials; and excessive power dissipation can lead to increases in the size and cost of the prime mover, as well as in associated manufacturing and operating costs [2]. Although it is clear that a design which minimizes momentum transport will be 'good', it is also clear that in many applications other criteria may be of equal importance, such as size, material cost, manufacturability, safety, and acoustic emission [3, 4].

A number of studies have been undertaken in the past that aim to optimize (or improve) heat removal with respect to various penalties, such as material and manufacturing cost [5], pressure drop [5, 6], and pumping power [5, 7]. Much of this previous work on transport optimization has focused on particular applications, and has addressed neither a general framework for optimization, nor a general theory for the physical phenomena that relate transport enhancement and dissipation. In this paper, we focus on these two fundamental aspects of optimal heat transfer design: the analysis of the optimization problem based on reduced variable 'universal' scalings; and the development of a basic understanding of the underlying physical transport phenomena so as to allow for *a priori* evaluation of the viability of a particular thermal-hydraulic design.

In Section 2 we define the channel flow configuration of interest and state the optimization problem. In Section 3 we solve the optimization problem in a formal sense, and relate the results via Reynolds' analogy to a general hydrodynamic stability criteria. In Section 4 we describe the experimental apparatus used to generate the thermal-hydraulic data required by the optimization procedure. Lastly, in Section 5, we present results of a channel optimization study based on several augmentation schemes, and demonstrate the significant savings possible through optimal design.

2. THE OPTIMIZATION PROBLEM

We consider the problem shown in Fig. 1 of incompressible flow in a plane channel of length L and

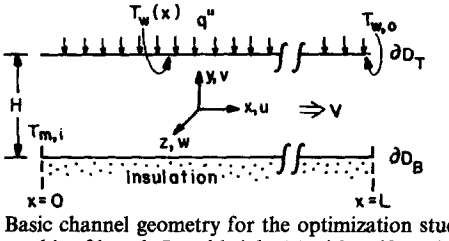

FIG. 1. Basic channel geometry for the optimization study. The channel is of length L and height H, with uniform heat flux q'' imposed on the top wall, ∂D_T, and an adiabatic bottom surface, ∂D_B.

NOMENCLATURE

a	groove length (Fig. 2(b))
A	area of the y–z channel cross section
b	distance of the eddy promoters from the top wall (Fig. 2(a))
B	constant in equation (A9a)
c	groove dwell (Fig. 2(b))
c_p	specific heat at constant pressure
C	constant in equation (A9b)
d	diameter of the eddy promoters (Fig. 2(a))
∂D_B	bottom wall surface (Fig. 1)
∂D_T	top wall surface (Fig. 1)
e	groove depth (Fig. 2(b))
f	friction factor defined by equation (11)
g	gravitational acceleration
$g(\mu)$	function defined by equation (A4)
$\tilde{g}(\mu)$	function defined by equation (A11)
H	channel height (Fig. 1)
k	thermal conductivity
l	distance between successive eddy-promoter cylinders (Fig. 2(a))
L	channel length (Fig. 1)
Nu	Nusselt number, $q''H/k\overline{\Delta T}$
ΔP	pressure drop
Pr	Prandtl number, ν/α
q''	heat flux per unit area
R	Reynolds number, VH/ν
t	time
T	temperature
δT	total temperature difference defined by equation (2)
$\overline{\Delta T}$	time-averaged temperature difference between wall temperature and mixed mean temperature of the fluid
u, v, w	velocity components in the x-, y- and z-directions, respectively
u_*	friction velocity, $\sqrt{(\tau_w/\rho)}$
$\mathbf{v}$	velocity vector
V	channel-average velocity defined by equation (1)
x, y, z	Cartesian coordinates
Y	set of fluid properties, $\{k, \rho c_p, \nu, \rho\}$
Z_n	set of geometric parameters for channel geometry n.

Greek symbols

α	thermal diffusivity, $k/\rho c_p$
β	constant in equation (A9b)
γ	Reynolds' analogy constant
ε	non-analogous momentum transfer coefficient in equation (14)
η	constant in equation (A9a)
λ	non-dimensional channel height, $q''H/k\delta T$
Λ	non-dimensional thermal load, $q''L/k\delta T$
μ	non-dimensional inverse velocity, $q''L/(k\delta TR\,Pr)$
ν	kinematic viscosity
ξ	constant in equation (A9b)
τ_w	shear stress at the wall
Ψ	non-dimensional dissipation parameter defined by equation (7).

Subscripts

c	critical
i	inlet
m	mixed mean
n	channel geometry
o	exit
tr	transition
w	wall
0	base geometry, smooth channel
1	periodic eddy-promoter channel
2	periodic microgrooved channel.

Superscripts

*	optimum
UB	upper bound.

height H, with uniform heat flux q'' imposed on the top wall ∂D_T, and an adiabatic bottom surface ∂D_B. The flow is assumed to be hydrodynamically and thermally fully developed in x, and independent (on average) of the spanwise coordinate z. The flow is forced by a pressure gradient $\Delta P/L$, resulting in a channel-average velocity of

$$V = \frac{1}{A}\int_{-\infty}^{\infty}\int_{-H/2}^{H/2}\langle u(x,y,z,t)\rangle\,dy\,dz \qquad (1)$$

where u is the x-component of the velocity, $\mathbf{v} = u\hat{\mathbf{x}} + v\hat{\mathbf{y}} + w\hat{\mathbf{z}}$, A the area of the y–z channel cross section, and $\langle\cdot\rangle$ refers to temporal average. The fluid is assumed to be characterized by constant (temperature-independent) properties given by the thermal conductivity k, the volumetric specific heat ρc_p, the kinematic viscosity ν, and the density ρ. Natural convection and all compressibility effects are assumed negligible. The set of physical properties will be denoted $Y = \{k, \rho c_p, \nu, \rho\}$.

In addition to the basic geometry in Fig. 1, we shall also consider two heat transfer enhancements corresponding to the addition of (a) periodic eddy promoters and (b) microgrooves, shown schematically in Figs. 2(a) and (b), respectively. The eddy promoters in Fig. 2(a) are adiabatic, and thus they effect the heat transfer only through flow modification. We shall denote the base geometry in Fig. 1 as Z_0, and describe the two enhancement geometries

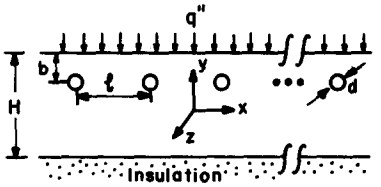

FIG. 2(a). The geometry of the periodic eddy-promoter channel is described by the distance between successive eddy-promoter cylinders, l, the diameter of the eddy promoters, d, and the distance of the eddy promoters from the top wall, b. The eddy-promoter cylinders are adiabatic.

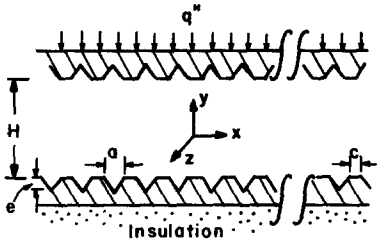

FIG. 2(b). The geometry of the periodic microgrooved channel is described by the depth of the groove, e, the groove length, a, and the groove dwell, c. The vertical scale of the grooves is greatly exaggerated for clarity.

by the sets Z_n, $Z_1 = \{d/H, b/H, l/H\}$ for the eddy promoters, and $Z_2 = \{e/H, a/H, c/H\}$ for the microgrooved channels. Here d is the eddy promoter cylinder diameter, b the distance between the eddy promoters and the top wall, and l the distance between successive cylinders in the array; e is the microgroove depth, a the groove length, and c the groove dwell. The geometries Z_0, Z_1, Z_2 are all periodic, and thus the concept of being fully developed is well defined [8, 9].

We now construct the minimum-dissipation transport problem associated with these geometries (we do not consider the minimum-stress and minimum-pressure-drop problems as they follow along similar lines). To begin, we write the temperature difference $\delta T = T_{w,o} - T_{m,i}$ as

$$\delta T = \frac{q'' L}{\rho c_p V H} + \overline{\Delta T} \tag{2}$$

where $T_{w,o}$ is the heated wall temperature at $x = L$, $T_{m,i}$ the mixed mean temperature of the fluid at the inlet ($x = 0$), and $\overline{\Delta T} = \langle \overline{T_w(x) - T_m(x)} \rangle$. Here the overbar refers to an average in x over length scales of the order of the periodic enhancement structures (l and a are assumed to be small compared to L). The mixed mean temperature $T_m(x)$ is given by

$$T_m(x) = \frac{1}{VA} \int_{-\infty}^{\infty} \int_{-H/2}^{H/2} \langle uT \rangle \, dy \, dz. \tag{3}$$

Note that temperature gradients across the channel walls are assumed negligible.

In terms of the above temperature difference we can now state the optimization problem as

$$\min_{V,H,Z_n} \{\Delta P V H\} \quad \text{for fixed } \{q'', \delta T, L, Y\} \tag{4}$$

where the parameter $\{\Delta P V H\}$ is the total viscous dissipation (pumping power) per unit width of the channel. Essentially, problem (4) requires that for a given thermal load, q'', that we find the flow velocity V, channel size H, and enhancement parameters Z_n that minimize the total dissipation for a fixed maximum wall temperature δT. We have chosen the wall temperature as our thermal constraint as this is the quantity that typically limits the structural integrity and performance of machinery or devices on the heated surface (e.g. computer chips [4, 6, 7]).

Optimization (4) corresponds to a multivariate constrained minimization problem, and inasmuch is rather difficult to solve. Furthermore, the relationship between the dissipation and the control and constraint variables will be highly nonlinear, requiring the solution of the full Navier–Stokes equation. Our approach to the problem consists of two parts: first, a non-dimensional scaling will be introduced that reduces the optimization problem to a 'universal' curve which can be obtained on the basis of standard thermal and hydraulic characterizations; second, a physical analysis will be developed that allows for *a priori* evaluation of the relative effectiveness of various Z_n as regards dissipation minimization.

3. SCALING ANALYSIS OF THE OPTIMIZATION PROBLEM

3.1. *Nondimensionalization*

To reduce problem (4) to a universal form we introduce a nondimensionalization in which only fixed constraint variables (*not* control variables) are used to scale length, time, and temperature. To start, we introduce a Prandtl number, a Reynolds number, and a Nusselt number

$$Pr = \nu/\alpha \tag{5a}$$

$$R = VH/\nu \tag{5b}$$

$$Nu(R, Pr; Z_n) = q'' H / k \overline{\Delta T} \tag{5c}$$

and a thermal load parameter

$$\Lambda = q'' L / k \delta T. \tag{6}$$

A non-dimensional dissipation parameter Ψ is defined as

$$\Psi = \frac{3^3 2}{5^5} \frac{\Delta P V H Pr^2 L^2}{\rho \nu^3}. \tag{7}$$

Lastly, we introduce two non-dimensional control parameters

$$\lambda = q'' H / k \delta T \tag{8}$$

$$\mu = q'' L / (k \delta T R Pr) \tag{9}$$

where λ is a non-dimensional channel height, and μ a non-dimensional inverse velocity. In terms of the non-dimensional variables, equations (5)–(9), the optimization problem (4) can be written as

$$\min_{\mu,\lambda,Z_n} \Psi \quad \text{for fixed } \{q'', \delta T, L, Y\} \tag{10a}$$

subject to the fixed δT constraint (2)

$$\lambda/Nu + \mu = 1. \tag{10b}$$

Note μ can be interpreted as the ratio of the difference between the fluid mixed mean temperature at the exit ($x = L$) and the inlet ($x = 0$), to the total temperature difference δT.

To proceed further we introduce the friction factor

$$f(R; Z_n) = \frac{(\Delta P/L)(H/2)}{(1/2)\rho V^2} \tag{11}$$

to write equation (7) as

$$\Psi = \frac{3^3 2}{5^5}\{f R^3 \Lambda^3 \lambda^{-3} Pr^2\}. \tag{12}$$

Finally, using the constraint $\lambda = Nu(1-\mu)$ and the relation $R = \Lambda/\mu Pr$ we arrive at the following problem:

$$\min_{\forall \mu \in [0,1], Z_n} \Psi(\mu, Z_n) = \frac{3^3 2}{5^5} \frac{\Lambda^6}{Pr} \frac{f(\Lambda/\mu Pr; Z_n)}{Nu^3(\Lambda/\mu Pr, Pr; Z_n)\mu^3(1-\mu)^3}. \tag{13}$$

Note that by 'optimal Z_n' we refer to both the choice of n and the choice of non-dimensional parameters within Z_n.

It can be seen from equation (13) that for a given Z_n the optimal operating conditions depend only on the Prandtl number Pr, the thermal load Λ, and the non-dimensional thermal ($Nu(R, Pr; Z_n)$) and hydraulic ($f(R; Z_n)$) behavior of the system. In practice, the optimization proceeds as follows:

(1) choose a fluid (Pr) and the thermal load (Λ);
(2) for each Z_n find μ_n^* such that

$$\Psi_n^* = \Psi(\mu_n^*, Z_n) < \Psi(\mu, Z_n) \forall \mu \in [0, 1];$$

(3) find Z_{n^*} such that

$$\Psi^* = \Psi(\mu_{n^*}^*, Z_{n^*}) < \Psi(\mu_n^*, Z_n) \forall Z_n.$$

The dimensional V and H are then determined as follows: μ implies R, Nu and hence λ; λ implies H; knowledge of H and R then gives the velocity V.

3.2. *General hydrodynamic considerations*

The above minimization for a given Z_n is relatively simple, and can be effected once one set of experimental measurements $Nu(R, Pr; Z_n)$, $f(R; Z_n)$ have been conducted (for *any* H). Unfortunately, the number of parameters in each Z_n, and the potentially large number of different Z_n (e.g. eddy promoters, microgrooves, flow oscillation [3, 10]) can lead to an intractable problem. It is thus clear that a broad theory relating hydrodynamic behavior and scalar transport is required in order to reduce the number of interesting enhancement geometries. To this end, we analyze our problem for the case of Reynolds' analogy flows [11, 12], in which we assume that

$$f(R; Z_n) = \frac{2\gamma\, Nu(R, Pr; Z_n)}{R} + \frac{\varepsilon(R; Z_n)}{R} \tag{14}$$

where γ is 'Reynolds' analogy constant' which should scale as $Pr^{-1/3}$ (and is a function only of Pr), and ε represents non-analogous momentum transfer [11]. Note that although equation (14) is perfectly general, it will only be useful for small ε/Nu. A detailed analysis of ε for transitional eddy promoter flows is given in ref. [11], in which the utility of expansion (14) is demonstrated.

We now insert equation (14) into equation (13), and neglect the $O(\varepsilon)$ term to reduce our minimization problem to

$$\min_{\forall \mu \in [0,1], Z_n} \Psi = \frac{3^3 2^2}{5^5} \frac{\gamma \Lambda^5}{Nu^2(\Lambda/\mu Pr, Pr; Z_n)} \frac{1}{\mu^2(1-\mu)^3}. \tag{15}$$

To get an upper bound for Ψ_n^*, Ψ_n^{*UB}, we neglect variations of Nu with μ to obtain (see the Appendix)

$$\Psi_n^{*UB} = \gamma \Lambda^5 Nu^{-2}(5\Lambda/2Pr, Pr; Z_n). \tag{16}$$

Assuming (plausibly) that Ψ_n^{*UB} and Ψ_n^* behave similarly, we can make the following conclusions as regards the relationship between enhancement and dissipation minimization. First, we see that an increase in Nu at fixed R (here $5\Lambda/2Pr$) by an enhancement Z_n *does* result in a decrease in dissipation Ψ (in fact a quadratic decrease), consistent with the conventional wisdom that an increase in $Nu(R)$ is in some sense 'good'. Note that for the minimum-stress and minimum-pressure-drop problems the results are similar, however, the reduction in these quantities is only linear in Nu^{-1}. Second, as the thermal load Λ increases, an enhancement procedure is required which modifies the Nusselt number at higher Reynolds numbers. In essence, equation (16) indicates that $5\Lambda/2Pr$ is roughly the Reynolds number at which the most important dissipation reduction can be achieved; increasing Nu at other Reynolds numbers will have a less significant effect.

Both of these conclusions can be interpreted in terms of our previous work on transport enhancement by flow destabilization [10, 11]. As regards the first point, the increase in Nu at fixed R is best considered as a decrease in the stability of the flow, that is, an increase in the correlated velocity–temperature fluctuations (perhaps better measured by a Stanton number than a Nusselt number). The enhancement problem then becomes one of maximizing destabilization while maintaining non-analogous momentum transport (ε in equation (14)) small; a detailed analysis of this problem for laminar unsteady eddy promoter flows is given in ref. [11]. As regards the second point, it is clear that once a flow is destabilized by some enhancement procedure Z_n at some critical Reynolds number R_c, for $R \gg R_c$ there will be significant non-

linear saturation: the relative increase in Nusselt number will decrease, and non-analogous drag will dominate. As Λ increases and the Reynolds number at which optimal enhancement occurs increases, new augmentation schemes Z_n must be effected to destabilize the new flow. As we know that with increasing R the range of naturally unstable scales increases (e.g. the energy cascade), this implies that with increasing Λ we require destabilization at smaller and smaller (intrinsically stable) spatial scales—in essence, *scale-matched destabilization.*

4. EXPERIMENTAL APPARATUS AND THERMAL-HYDRAULIC DATA

To demonstrate the utility and validity of the optimization procedures and physical arguments described in the previous sections, we have conducted a series of experiments for the geometries Z_0, Z_1, Z_2 shown in Figs. 1 and 2. The experiments were carried out in air ($Pr = 0.71$) in a low-turbulence wind tunnel; details of the Z_1 and Z_2 test sections are presented in Figs. 3 and 4, respectively. The only cases studied in this paper are Z_0, $Z_1 = \{d/H = 0.2,\ b/H = 0.25,\ l/H = 3.33\}$, and $Z_2 = \{e/H = 0.025,\ a/H = 0.035,\ c/H = 0.015\}$. The ratio of the width of the channel W, to the channel height H is $W/H = 9.0$, which is considered sufficiently large that the results can be considered close to those for an 'infinite' planar channel; the friction factor data presented are further corrected by subtracting out the shear stress at the side walls. The channel is fitted with electrical strip heaters on the top channel wall to deliver the necessary uniform heat flux q''.

For the optimization studies of interest we require a set of f, Nu data for each Z_n. A single H is chosen, and the flow rate is varied to achieve a range of Reynolds numbers. For each Reynolds number the pressure drop and fluid and wall temperatures are measured, thus allowing the $f(R; Z_n)$ and $Nu(R, Pr; Z_n)$ curves to be constructed. The pressure drop is measured with an MKS Baratron differential pressure transducer, and the flow rate is calculated from pitot-static velocity measurements at outflow. Temperature measurements are made using copper–constantan thermocouples. All measurements are deemed accurate to the 10% necessary for the optimization studies undertaken.

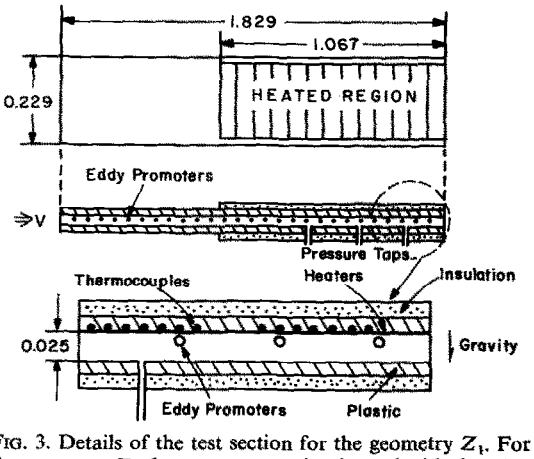

FIG. 3. Details of the test section for the geometry Z_1. For the geometry Z_0 the same test section is used with the eddy promoters removed. All units are in meters.

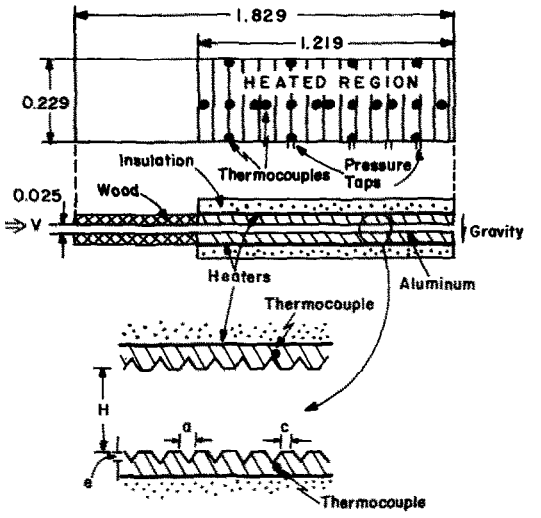

FIG. 4. Details of the test section for the geometry Z_2. The inner walls in the heated region are made of high conductivity aluminum to insure that the temperature difference between the thermocouples and the grooved surface is small. The microgrooves are machined on the aluminum plates to high precision using a shaper. All units are in meters.

Lastly, we note that the flow is allowed to become thermally fully developed in the streamwise direction x before any measurements are taken. All measurements are taken after a distance of roughly $55H$ from the inlet of the channel, and roughly $35H$ from the beginning of the heated region. The resulting entrance regions are sufficient to obtain hydraulically and thermally fully-developed flat-channel laminar flows for Reynolds numbers $R < 800$, and fully-developed flat-channel turbulent flows for Reynolds numbers $R > 5500$ [13]. The entrance length for the geometries Z_1, Z_2 will be much shorter than for the smooth channel Z_0 as a result of destabilization. In addition to these theoretical considerations of entrance-length effects, it has also been verified directly from measurement that both the (time-average) wall pressure and temperature vary linearly with x, consistent with fully developed flow.

We plot in Figs. 5 and 6 the $f(R; Z_n)$ and $Nu(R, Pr = 0.71; Z_n)$ curves for the geometries Z_0, Z_1, Z_2 that will be used in the optimization studies that follow. We supplement our new data with analytical solutions [14] and numerical solutions [11] at lower Reynolds numbers, and previous experimental correlations and power laws at higher Reynolds numbers [14]. The Nusselt number data obtained from $Pr = 1$ numerical solutions [11] are corrected for the Prandtl number of interest here ($Pr = 0.71$) assuming

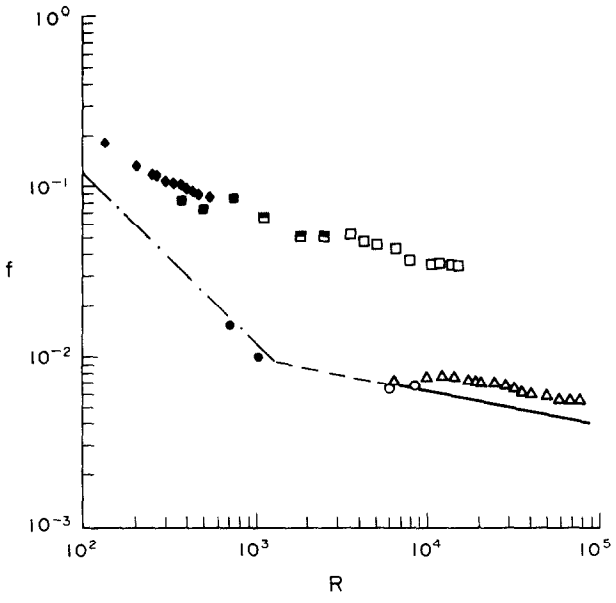

FIG. 5. Friction coefficient data. Z_0 (smooth channel): ○, experiment; —·—, laminar analytical solution $f = 12/R$; ——, turbulent correlation $f = 0.040/R^{0.2}$ [14] (the dashed line indicates the Reynolds number range for which the correlation is somewhat suspect). Z_1 (eddy promoters): □, experiment; ◇, numerical [11]. Z_2 (microgrooves): △, experiment. In all cases the solid symbols refer to laminar (steady or unsteady) flows, and the open symbols refer to turbulent flows. Note the 'premature' drag crisis (■) in the Z_1 eddy-promoter geometry when the channel flow becomes turbulent at $R = R_{tr} \sim 1300$.

a Prandtl number power law dependence on enhancement as given in ref. [10]. Note that for purposes of approximate optimization we have extended the turbulent correlations for f and Nu down to the transitional Reynolds number, $R_{tr} = 1300$, although it is clear that the correlations are strictly valid only at somewhat larger R. The suspect region of the correlation is indicated by a dashed line.

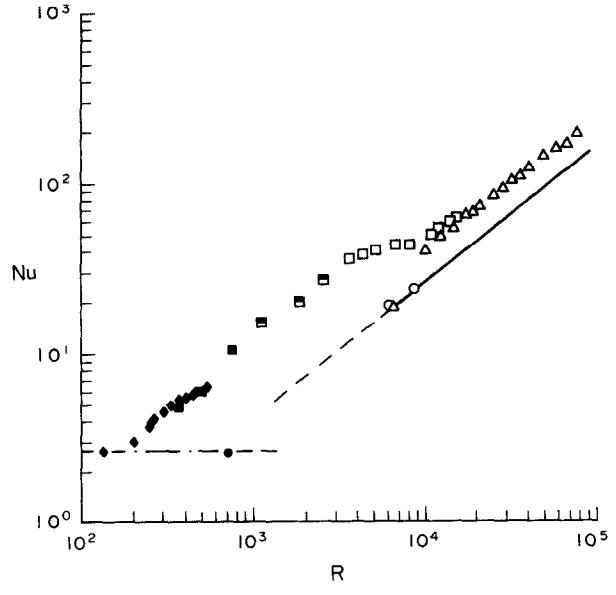

FIG. 6. Heat transfer data for $Pr = 0.71$. Z_0 (smooth channel): ○, experiment; —·—, laminar analytical solution $Nu = 2.70$; ——, turbulent correlation $Nu = 0.020R^{0.8}\,Pr^{0.4}$ [18] (the dashed line indicates the Reynolds number range for which the correlation is somewhat suspect). Z_1 (eddy promoters): □, experiment (■ indicates transitional drag crisis); ◇, numerical [11]. Z_2 (microgrooves): △, experiment. In all cases the solid symbols refer to laminar (steady or unsteady) flows, and the open symbols refer to turbulent flows.

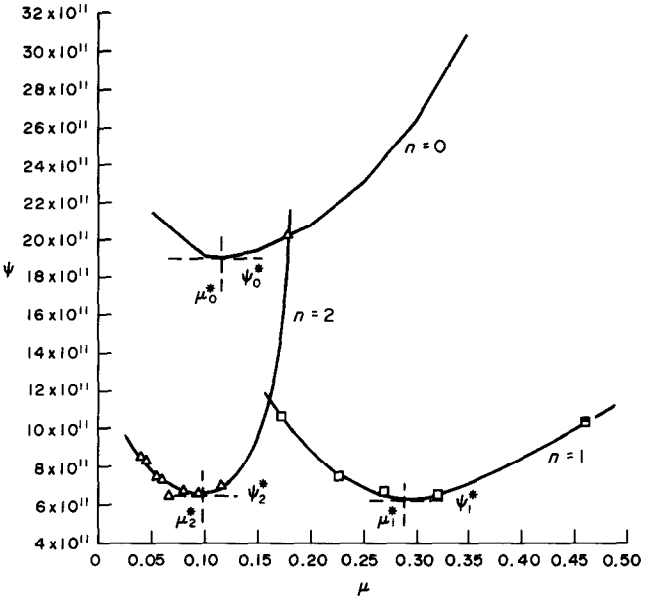

FIG. 7. A plot of $\Psi(\mu, Z_n)$ for a fixed thermal load of $\Lambda = 800$ based on the data sets of Figs. 5 and 6. The minimum of $\Psi(\mu, Z_n)$ for each Z_n curve gives one point Ψ_n^* ($\Lambda = 800$) in Fig. 8. Note that from μ_n^* we can find the optimizing channel height H and flow velocity V.

The experiments for the microgrooved channel were, in fact, carried out for heating and microgrooves, on *both* channel walls, as shown in Fig. 4. To construct one-sided heating/microgrooved data from these experiments we assume that $Nu_{1\text{-sided}} \simeq Nu_{2\text{-sided}}$, and that $f_{1\text{-sided}} \simeq 1/2[f_{2\text{-sided}} + f(\cdot\,; Z_0)]$, where $f(\cdot\,; Z_0)$ refers to the friction factor in the flat-channel geometry Z_0. This approximation appears reasonable for the small e/H considered here.

5. OPTIMIZATION RESULTS

We present here results of the optimization procedure developed in Section 3 based on the data of

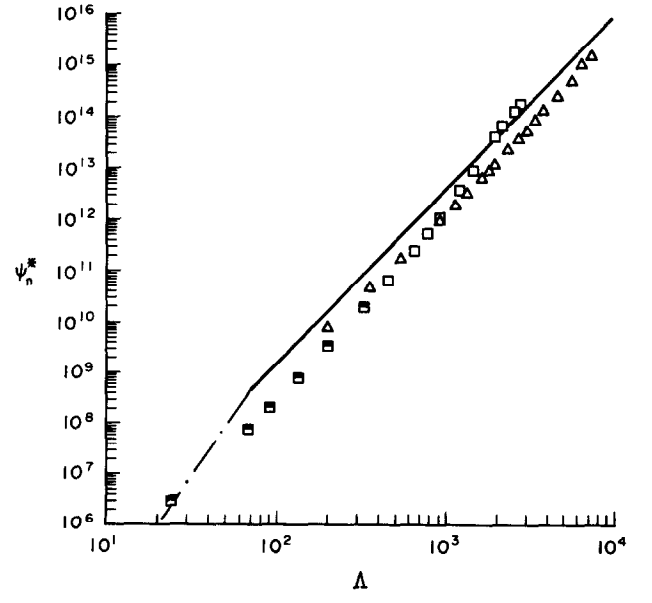

FIG. 8. A plot of $\Psi_n^*(\Lambda)$ for Z_0, Z_1, and Z_2 based on the data sets of Figs. 5 and 6. Z_0 (smooth channel); —·—, global optimum corresponds to laminar flow; ——, global optimum corresponds to turbulent flow. Z_1 (eddy promoters): □, experiment (■ indicates transitional drag crisis). Z_2 (microgrooves): △, experiment.

Section 4. In Fig. 7 we plot $\Psi(\mu, Z_n)$ for a fixed $\Lambda = 800$ and Z_0, Z_1, Z_2, while in Fig. 8 we plot $\Psi_n^*(\Lambda)$ for the geometries Z_0, Z_1, Z_2. Figure 7 demonstrates how Fig. 8 is constructed; the minimum of each Z_n curve in Fig. 7 results in one point (at $\Lambda = 800$) on Fig. 8, as described by the optimization procedure outlined at the end of Section 3.1. For the cases of laminar flat-channel flow and power-law correlation turbulent flat-channel flow the minimization over μ for each Λ can be carried out analytically, as summarized in the Appendix. It can be seen from Fig. 7 that for a given geometry Z_n, operating at a non-optimal μ can significantly increase the dissipation; this illustrates the importance of optimization even for the case of 'unenhanced' heat transfer.

Figure 8 demonstrates that the scale-matched destabilization theory proposed in Section 3 is, indeed, valid. First, it is seen from Fig. 8 that for very low Λ, Z_0 laminar flow performs the best, as the Λ–R matching (Section 3) insures that enhancement can have little effect. Second, as Λ increases, the macroscale eddy promoters Z_1 becomes relatively more efficient than flat channels Z_0; this is due to the fact that the eddy promoters destabilize the flow and increase the Nusselt number, thereby decreasing dissipation by equation (16). The fact that ε in equation (14) is small for these flows despite significant destabilization is due to the fact that channel flows are only viscously (slightly) stable, as described in detail in ref. [11]. Note that the transitional eddy-promoter flows are optimal over a broad range of Λ due to the beneficial effect of the premature cylinder drag crisis; in fact, it appears that laminar eddy promoters are never selected, as they are bettered at low Λ by laminar Z_0 flow, and at higher Λ by transitional eddy promoters.

Third, as Λ increases even further, eddy promoters are no longer efficient at destabilizing the flow at $R \sim \Lambda$ (the necessary R for destabilization according to equation (16)), due to the fact that the eddy-promoter macroscales are themselves naturally unstable at this turbulent Reynolds number. It is at this point that the microgrooves become important, as they match the 'stable' part of the flow, the viscous sublayer [15]. The microgrooves become important at $u_* e/\nu \cong 30$ (implying $R \cong 16\,666$ and thus $\Lambda \cong 1400$), consistent with past studies on the effect of roughness in transport processes. Here u_* is the friction velocity, which is defined as $u_* = \sqrt{(\tau_w/\rho)}$, where τ_w is the shear stress at the wall. (Details of the physics of our regular two-dimensional uniform roughness as compared to 'sand grain' roughness [16] are given elsewhere [17].) Note the savings due to flow destabilization at low Λ appear to be larger than those at high Λ; although this may reflect the intrinsic instability of turbulent flows, it may also be due to a non-optimized microgroove surface.

There is a great deal of information in Fig. 8 as regards the scaling of minimum dissipation with thermal load. For instance, if Λ is increased from 10^2 to 10^3 (due to, say, a decrease in the allowable δT by a factor of 10), the dimensional minimum dissipation $\{\Delta P V H\}^* \sim \Psi^*$ increases by roughly a factor of 10^3; this illustrates the rather severe penalty associated with stringent thermal load requirements. If we assume that $Nu \sim R^\beta$, it follows from Reynolds' analogy argument and upper bound (16) that the minimum dissipation Ψ^* scales as $\Psi^* \sim \Lambda^{5-2\beta}$, which is consistent with the data of Fig. 8 for a (physically plausible) value of β slightly less than unity.

Much work remains to be done on understanding the detailed physics of both the macroscale and microscale destabilization [11, 17], as well as on extending the optimization procedures described here to include non-fully developed effects, inlet and exit effects, and more complicated configurations [17]. These extensions are relegated to other papers: our primary focus in the current paper is on the scaling of the minimum-dissipation optimization problem, and on understanding the relationship between the physics of transport enhancement and dissipation minimization.

Acknowledgements—We would like to thank Dr George Em Karniadakis for contributions to this work. This work was supported by the NSF under Grant CBT 85-06146, and by the ONR and DARPA under Contract N00014-85-K-0208.

REFERENCES

1. B. J. Bellhouse, F. H. Bellhouse, C. M. Curl, T. I. Macmillan, A. J. Gunning, E. H. Spratt, S. B. MacMurray and J. M. Nelems, A high efficiency membrane oxygenerator and pulsative pumping system, and its application to animal trials, *Trans. Am. Soc. Artif. Internal Organs* **19**, 77 (1973).
2. M. S. Isaacson and A. A. Sonin, Sherwood number and friction factor correlations for electrodialysis systems, with application to process optimization, *I&EC Process Des. Dev.* **15**, 313 (1976).
3. A. E. Bergles, Techniques to augment heat transfer. In *Handbook of Heat Transfer Applications* (Edited by W. M. Rohsenow, J. P. Hartnett and E. N. Ganic). Chap. 3. McGraw-Hill, New York (1986).
4. W. Nakayama, Thermal management of electronic equipment: a review of technology and research topics, *Appl. Mech. Rev.* **39**(12), 1847 (1986).
5. R. L. Webb and A. E. Bergles, Performance evaluation criteria for selection of heat transfer surface geometries used in low Reynolds number heat exchangers. In *Low Reynolds Number Flow Heat Exchangers* (Edited by S. Kakac, R. K. Shah and A. E. Bergles), p. 735. Hemisphere, Washington, DC (1983).
6. D. B. Tuckerman and R. F. W. Pease, High performance heat sinking for VLSI, *IEEE Electron Device Lett.* **EDL-2**(5), 126 (1981).
7. D. B. Tuckerman, Heat transfer microstructures for integrated circuits, Ph.D. Thesis, Electrical Engineering Department, Stanford University (1984).
8. N. K. Ghaddar, G. E. Karniadakis and A. T. Patera, A conservative isoparametric spectral element method for forced convection; application to fully developed flow in periodic geometries, *Numer. Heat Transfer* **9**, 277 (1986).
9. S. V. Patankar, C. H. Liu and E. M. Sparrow, Fully developed flow and heat transfer in ducts having streamwise-periodic variations of cross-sectional area, *J. Heat Transfer* **99**, 180 (1977).
10. N. K. Ghaddar, M. Magen, B. B. Mikic and A. T.

Patera, Numerical investigation of incompressible flow in grooved channels. Part 2: resonance and oscillatory heat transfer, *J. Fluid Mech.* **168,** 541 (1986).
11. G. E. Karniadakis, B. B. Mikic and A. T. Patera, Minimum dissipation transport enhancement by flow destabilization: Reynolds' analogy revisited, *J. Fluid Mech.* **192,** 365 (1988).
12. O. Reynolds, On the extent and action of the heating surface for steam boilers, *Proc. Manchr Lit. Phil. Soc.* **14,** 7 (1874).
13. H. Schlichting, *Boundary Layer Theory*. McGraw-Hill, New York (1968).
14. W. M. Kays and M. E. Crawford, *Convective Heat and Mass Transfer*. McGraw-Hill, New York (1980).
15. H. Tennekes and J. L. Lumley, *A First Course in Turbulence*. MIT Press, Cambridge, Massachusetts (1972).
16. D. F. Dipprey and R. H. Sabersky, Heat and momentum transfer in smooth and rough tubes at various Prandtl numbers, *Int. J. Heat Mass Transfer* **14,** 601 (1963).
17. H. Kozlu, Ph.D. Thesis, Department of Mechanical Engineering, MIT, in progress.
18. W. M. Rohsenow and H. Choi, *Heat, Mass and Momentum Transfer*. Prentice-Hall, Englewood Cliffs, New Jersey (1961).

APPENDIX

We consider here three cases in which the optimization problem (13)

$$\Psi^*(\mu^*) < \Psi(\mu) = \frac{3^3 2}{5^5}\frac{\Lambda^6}{Pr}\frac{f(\Lambda/\mu\, Pr)}{Nu^3(\Lambda/\mu\, Pr)\mu^3(1-\mu)^3} \quad \forall \mu \in [0,1] \tag{A1}$$

can be 'solved' in closed form. The three flows amenable to analytical treatment are: Reynolds' analogy flows; laminar flat-channel flow; and turbulent flat-channel flow. These exact optimizations are interesting not only in terms of the results they produce, but also in terms of the insight they give into the optimization procedure.

Reynolds analogy flow upper bound

Here we assume that equation (14) holds with $\varepsilon = 0$

$$f(R) = \frac{2\gamma\, Nu}{R} \tag{A2}$$

for which expression (A1) can then be written as

$$\Psi(\mu) = \frac{3^3 2^2}{5^5}\frac{\gamma\Lambda^5}{Nu^2(\Lambda/\mu\, Pr, Pr)}\frac{1}{\mu^2(1-\mu)^3}. \tag{A3}$$

To proceed further we construct an *upper* bound for the minimum of $\Psi(\mu)$ by neglecting the variation of Nu with μ and minimizing the function

$$g(\mu) = [\mu^2(1-\mu)^3]^{-1} \mu \in [0,1]. \tag{A4}$$

It is readily shown that $g(2/5) \leqslant g(\mu)$ for all $\mu \in [0,1]$, from which it directly follows that

$$\mu^{*UB} = 2/5 \tag{A5a}$$

$$\Psi^{*UB} = \gamma\Lambda^5\, Nu^{-2}(5\Lambda/2Pr, Pr). \tag{A5b}$$

This result is used extensively in the paper to motivate the concept of scale-matched destabilization.

Laminar flat-channel flow

For laminar flat channel flow we have the exact solutions [14]

$$f = 12/R \tag{A6a}$$

$$Nu = 2.70 \tag{A6b}$$

giving for $\Psi(\mu)$

$$\Psi(\mu) = \frac{3^3 2}{5^5}\frac{12\Lambda^5}{(2.70)^3}\frac{1}{\mu^2(1-\mu)^3}. \tag{A7}$$

From our previous analysis of Reynolds' analogy flows it is clear that if we minimize equation (A7) over all $\mu \in [0, 1]$ that we will obtain $\mu^* = 2/5$, $\Psi^* = 0.305\Lambda^5$.

The result $\Psi^* = 0.305\Lambda^5$ is only valid for a limited range of Λ, as laminar flow can only occur for $R < R_{tr}$. (We take R_{tr} here to be $R_{tr} = 1300$; although R_{tr} can be larger than this value in quiet experiments, in most engineering situations $R_{tr} = 1300$ is a very good predictor of transition.) This implies from equation (9) that we should minimize $\Psi(\mu)$ only for $(\Lambda/R_{tr}\, Pr) < \mu < 1$. If $(\Lambda/R_{tr}\, Pr) < 2/5$ our previous result holds, $\mu^* = 2/5$, $\Psi^* = 0.305\Lambda^5$, however, if $(\Lambda/R_{tr}\, Pr) > 2/5$ the minimum Ψ now occurs at the endpoint $\mu = \Lambda/R_{tr}\, Pr$. Our final result for laminar flow is therefore

$$0 < \Lambda < \frac{2R_{tr}\, Pr}{5} = 369.2 \quad \mu^* = 2/5$$

$$\Psi^* = 0.305\Lambda^5 \tag{A8a}$$

$$369.2 < \Lambda < R_{tr}\, Pr = 923 \quad \mu^* = \Lambda/923$$

$$\Psi^* = \frac{8975.05\Lambda^3}{(1-(\Lambda/923))^3} \tag{A8b}$$

where the numerical values given are for $Pr = 0.71$, $R_{tr} = 1300$. No laminar solution exists for $\Lambda > R_{tr}\, Pr$, as in this case the mixed-mean temperature rise *alone* is greater than the allowable δT. Note that as Λ approaches the limiting value $R_{tr}\, Pr$ the dissipation goes to infinity, as VH is finite but H goes to zero.

Turbulent flat-channel flow

We assume here power law correlations for the friction factor and Nusselt number

$$f = BR^{\eta} \tag{A9a}$$

$$Nu = CR^{\beta}\, Pr^{\xi} \tag{A9b}$$

giving

$$\Psi(\mu) = \frac{3^3 2}{5^5}\frac{B}{C^3}\frac{\Lambda^{6+\eta-3\beta}}{Pr^{1+\eta+3\xi-3\beta}}\frac{1}{\mu^{3+\eta-3\beta}(1-\mu)^3}. \tag{A10}$$

Defining the function $\tilde{g}(\mu)$ as

$$\tilde{g}(\mu) = [\mu^{3+\eta-3\beta}(1-\mu)^3]^{-1} \tag{A11}$$

it can be readily shown that for $\mu^* = (3+\eta-3\beta)/(6+\eta-3\beta)$, $\tilde{g}(\mu^*) \leqslant g(\mu)\, \forall\, \mu \in [0,1]$, from which the corresponding minimum dissipation can be calculated from equation (A10) as $\Psi^* = \Psi(\mu^*)$.

For turbulent flow in the channel shown in Fig. 1 we have $B = 0.04$, $\eta = -0.2$, $C = 0.02$, $\beta = 0.8$, $\xi = 0.4$ [14, 18], for which we obtain

$$\mu^* = 2/17 \tag{A12a}$$

$$\Psi^* = 258.14\Lambda^{3.4} \tag{A12b}$$

where the numerical value in equation (A12b) is for $Pr = 0.71$. The value of $\mu^* = 2/17$ for turbulent flow is less than the corresponding value (A8a) $\mu^* = 2/5$ for a laminar flow, implying that for optimal-performance turbulent flow relatively more of the temperature rise should be lateral as opposed to streamwise.

Turbulent flows can only exist for $R > R_{tr} \Rightarrow \mu < (\Lambda/R_{tr}\, Pr)$, and thus equations (A12) are, in fact, only valid for $(\Lambda/R_{tr}\, Pr) > 2/17$. To be more precise for lower Λ an 'endpoint' analysis similar to that used for laminar flow should be performed, the detail of which we do not present here. Note that the actual flat-channel minimization summarized in Fig. 8 represents the minimum over both laminar and turbulent flows, with endpoint extrema taken into account.

ENLEVEMENT DE CHALEUR AVEC DISSIPATION MINIMALE PAR DESTABILISATION CONTROLEE DE L'ECOULEMENT

Résumé—On considère l'enlèvement convectif de chaleur, à dissipation minimale, sur une paroi par un fluide avec déstabilisation de l'écoulement. On développe un schéma universel pour le problème d'optimisation et on montre à partir des arguments liés à l'analogie de Reynolds et à la stabilité hydrodynamique que la solution du transport à dissipation minimale correspond à la déstabilisation d'écoulement à un nombre de Reynolds (et une échelle spatiale associée) qui augmente (diminue) quand la charge thermique croît. Les économies significatives de dissipation sont montrées possibles dans une étude simple d'optimisation pour le transfert de chaleur dans un canal, à partir de données expérimentales pour différentes procédures d'accroissement. Le schéma d'optimisation de l'augmentation de transport va depuis les promoteurs de turbulence à macroéchelle jusqu'aux éléments de rugosité à microsillon, avec des charges thermiques croissantes, ce que vérifie la validité de la présente théorie.

MINIMALE ABFUHR VON DISSIPATIONSWÄRME DURCH STRÖMUNGSDESTABILISIERUNG

Zusammenfassung—Es wird die Minimierung der konvektiven Dissipationswärmeabfuhr von einer Wand an ein strömendes Fluid untersucht, wobei eine destabilisierende Strömungsbeeinflussung in Erwägung gezogen wird. Eine allgemeingültige Einteilung für die Problemoptimierung wird entwickelt. Über die Reynoldsanalogie zu den hydrodynamischen Stabilitätskriterien wird gezeigt, daß die dissipationsminimierende Lösung des Transportproblems, bei steigender thermischer Last (gegebene Reynoldszahl und entsprechende räumliche Größenordnung) mit einer steigenden Strömungsdestabilisation in Einklang steht. Durch eine, auf experimentelle Daten gestützte, Optimierungsstudie wird mit Hilfe verschiedener Maßstabsvergrößerungen die signifikante Verminderung der Reibungsverluste am Beispiel des Wärmeübergangs an einem Kanal nachgewiesen. Die optimale Maßstabsvergrößerung für die Transportvorgänge wird benutzt, um bei steigender thermischer Last von makroskopischen Wirbelerzeugern auf Elemente mit Micro-Rauhigkeiten zu schließen und hierdurch die Richtigkeit der Destabilisationstheorie zu beweisen.

ТЕПЛООТВОД С МИНИМАЛЬНОЙ ДИССИПАЦИЕЙ, ОРГАНИЗОВАННОЙ ПУТЕМ ВВЕДЕНИЯ В ПОТОК ВОЗМУЩЕНИЙ СООТВЕТСТВУЮЩЕГО МАСШТАБА

Аннотация—Рассматривается конвективный отвод тепла от стенки к потоку жидкости с минимальным рассеянием при внесении в поток возмущений соответствующего масштаба. Разработана универсальная техника нормировки для проблемы оптимизации, и на основе аналогии Рейнольдса и соображений гидродинамической устойчивости показано, что решение для случая минимального рассеяния соответствует дестабилизации потока при числе Рейнольдса (и соответствующем пространственном масштабе), которое возрастает (уменьшается) с увеличением тепловой нагрузки. На основе экспериментальных данных, полученных при исследовании переноса тепла в канале, показана возможность значительного снижения рассеяния для нескольких вариантов интенсификации переноса. Показано, что при увеличении тепловой нагрузки интенсификацию переноса определяют сначала макромасштабные вихри, а затем элементы микроструктурной шероховатости.